ELSEVIER

Journal of Quantitative Spectroscopy & Radiative Transfer 90 (2005) 191–206

Journal of Quantitative Spectroscopy & Radiative Transfer

www.elsevier.com/locate/jqsrt

WWW scattering matrix database for small mineral particles at 441.6 and 632.8 nm

H. Volten[a,b,*], O. Muñoz[c], J.W. Hovenier[a], J.F. de Haan[d], W. Vassen[e], W.J. van der Zande[b,f], L.B.F.M. Waters[a,g]

[a] *University of Amsterdam, Astronomical Institute "Anton Pannekoek", Kruislaan 403, Amsterdam 1098 SJ, The Netherlands*

[b] *Atmospheric Photophysics, FOM-Institute AMOLF, Kruislaan 407, Amsterdam 1098 SJ, The Netherlands*

[c] *Instituto de Astrofísica de Andalucía, CSIC, c/Camino Bajo de Huétor 24, Apartado 3004, Granada 18080, Spain*

[d] *KNMI, P.O. Box 201, De Bilt 3730 AE, The Netherlands*

[e] *Faculty of Exact Sciences, Free University, De Boelelaan 1081, Amsterdam NL-1081, The Netherlands*

[f] *Department of Molecular and Laser Physics, University of Nijmegen, Nijmegen 6252 ED, The Netherlands*

[g] *Instituut voor Sterrenkunde, Katholieke Universiteit Leuven, Celestijnenlaan 200D, Heverlee B-3001, Belgium*

Received 3 September 2003; accepted 13 March 2004

Abstract

We present a new extensive database containing experimental scattering matrix elements as functions of the scattering angle measured at 441.6 and 632.8 nm for a large collection of micron-sized mineral particles in random orientation. This unique database is accessible through the World-Wide Web. Size distribution tables of the particles are also provided, as well as other characteristics relevant to light scattering. The database provides the light scattering community with easily accessible information that is useful, for a variety of applications such as testing theoretical methods, and the interpretation of measurements of scattered radiation. To illustrate the use of the database, we consider cometary observations and compare them with (1) cometary analog data from the database, and (2) with results of Mie calculations for homogeneous spheres, having the same refractive index and size distribution as those of the analog data.

Keywords: Database; Light scattering; Irregular particles; Aerosols; Polarization

* Corresponding author. University of Amsterdam, Astronomical Institute "Anton Pannekoek", Kruislaan 403, Amsterdam 1098 SJ, The Netherlands. Tel.: +31-205257491; fax: +31-205257484.

E-mail address: hvolten@science.uva.nl (H. Volten).

0022-4073/$ - see front matter © 2004 Elsevier Ltd. All rights reserved.
doi:10.1016/j.jqsrt.2004.03.011

1. Introduction

Light scattering by small irregular particles occurs in many natural and artificial environments. Nowadays a considerable number of light scattering codes are available on the internet for such particles, often organized conveniently in databases. However, databases containing experimental light scattering results for natural irregular particles are scarce. In this article we introduce and discuss the contents of a database of experimental results with possible applications of the data. In recent years a considerable amount of experimental single scattering matrices as functions of the scattering angle obtained with the light scattering facility in Amsterdam [1,2] have become available for samples of randomly oriented small mineral particles in air with broad ranges of sizes and shapes [3–7]. From these data it has become clear that particle shape is highly important in determining the overall light scattering behavior of these samples. This has important implications. For example, it confirms that the use of Mie calculations to interpret data involving light scattering by irregular particles in such different media as comets, circumstellar and interstellar matter, or the Earth atmosphere, is often unlikely to give accurate results (see e.g. [8,9]).

To provide an incentive for further research and applications we have decided to make our experimental data more easily available for the light scattering community by storing our data in digital form in a database freely accessible through the Internet at http://www.astro.uva.nl/scatter as of September 2003. All data in this database have been previously published in scientific journals predominantly in graphical form [3–6]. The database contains the following data for several samples of mineral aerosols in random orientation:

- Tables of scattering matrix elements as functions of the scattering angle from 5° to 173° at two wavelengths, 441.6 and 632.8 nm.
- Tables of size distributions as measured with a laser diffraction method.
- Scanning electron microscope (SEM) images of the particles that are indicative of their shape characteristics.
- Information about the origin, color, composition, and/or the complex refractive index of the samples, when available.

We provide information on the accuracy of the data whenever available. We intend to update this database regularly with new measured scattering matrix results.

2. Scattering matrix elements

The heart of the database is the collection of the measured scattering matrix elements listed as functions of the scattering angle at two different wavelengths. Scattering matrices contain all polarizing properties of the samples of randomly oriented particles and play an important role in radiative transfer processes. If the incident light is unpolarized only a few elements of the scattering matrix (the first column) suffice to fix the flux and state of polarization of the light scattered once by the sample. But the complete scattering matrix is indispensable for accurate multiple scattering calculations, since even unpolarized light becomes polarized after being scattered.

For the definition of the scattering matrix we make use of the fact that the flux and polarization of a quasi-monochromatic beam of light can be represented by a column vector $\mathbf{I} = \{I, Q, U, V\}$,

which is called the Stokes vector [10,11]. If light is scattered by a sample of randomly oriented particles and time reciprocity applies, as is the case in our experiment, the Stokes vectors of the incident beam and the scattered beam are related by a 4×4 scattering matrix, for each scattering angle θ, as follows [10, Section 5.22]:

$$\begin{pmatrix} I_{\mathrm{sca}} \\ Q_{\mathrm{sca}} \\ U_{\mathrm{sca}} \\ V_{\mathrm{sca}} \end{pmatrix} = \frac{\lambda^2}{4\pi^2 D^2} \begin{pmatrix} F_{11} & F_{12} & F_{13} & F_{14} \\ F_{12} & F_{22} & F_{23} & F_{24} \\ -F_{13} & -F_{23} & F_{33} & F_{34} \\ F_{14} & F_{24} & -F_{34} & F_{44} \end{pmatrix} \begin{pmatrix} I_{\mathrm{inc}} \\ Q_{\mathrm{inc}} \\ U_{\mathrm{inc}} \\ V_{\mathrm{inc}} \end{pmatrix}, \tag{1}$$

where the subscripts inc and sca refer to the incident and scattered beams, respectively, λ is the wavelength, and D is the distance from the particles to the detector. The matrix, $\mathbf{F}$, with its dimensionless elements F_{ij} is called the scattering matrix of the sample and refers to light that has been scattered once. Its elements depend on the scattering angle, but not on the azimuthal angle. Here the plane of reference is the scattering plane, i.e., the plane containing the incident and the scattered light. It follows from Eq. (1) that there are in general 10 different matrix elements.

For unpolarized incident light, $F_{11}(\theta)$ is proportional to the flux of the scattered light and is also called scattering function or phase function. The ratio $-F_{12}(\theta)/F_{11}(\theta)$ equals the degree of linear polarization of the scattered light if the incident light is unpolarized and $F_{13}(\theta) = 0$. Note further that we must have $|F_{ij}(\theta)/F_{11}(\theta)| \leqslant 1$ [12].

In the database, all elements, except $F_{11}(\theta)$, are given relative to $F_{11}(\theta)$, i.e., we list $-F_{12}(\theta)/F_{11}(\theta)$, $F_{22}(\theta)/F_{11}(\theta)$, $F_{34}(\theta)/F_{11}(\theta)$, $F_{33}(\theta)/F_{11}(\theta)$, and $F_{44}(\theta)/F_{11}(\theta)$. Further, the values of $F_{11}(\theta)$ are normalized so that they equal one for $\theta = 30°$. In addition to each measured matrix element (ratio) value, the experimental (1-sigma) error is given. We refrained from listing the four element ratios $F_{13}(\theta)/F_{11}(\theta)$, $F_{14}(\theta)/F_{11}(\theta)$, $F_{23}(\theta)/F_{11}(\theta)$, and $F_{24}(\theta)/F_{11}(\theta)$, since we verified that these ratios never differ from zero by more than the experimental errors (see also [2]). This is consistent with scattering samples consisting of randomly oriented particles with equal amounts of particles and their mirror particles [10].

The scattering matrices given in the database satisfy the Cloude (coherency matrix) test [13] within the accuracy of the measurements [3–5].

Different conventions are occasionally used for Stokes parameters and, consequently, for the sign of the matrix element $F_{34}(\theta)$. The convention employed here is in accordance with [10] and [11].

3. Samples

The particle samples included in the database in September 2003 comprise a wide range in origin and composition, and have relevance for different subjects. They are named Feldspar, Red clay, Quartz, Loess, Pinatubo, Lokon, and Sahara [3]; Allende, Olivine S, M, L, and XL [4]; Green clay, Fly ash [5]; and El Chichon [6]. Pinatubo, Lokon, and El Chichon are volcanic ashes named after the pertinent volcano. Sahara is a sample of sand collected in the Saharan desert. Allende is material from the Allende meteorite. Fly ash consists of particles produced in a combustion process. The rest of the samples are named after their main mineral component or their geological classification. For

all samples (estimates of the) refractive indices, measurements of the size distributions, and one or two SEM images per sample are given in the database and will be discussed in the next section.

The samples differ in origin. Some have been collected from the ground in powdered form, which resulted for example, from natural erosion processes. Others were obtained by crushing larger rocks (e.g. Feldspar, Quartz, Olivine, Allende, Pinatubo). Several samples have been sieved to obtain different size distributions (e.g. Olivine) or to remove particles larger than about 100 μm in radius (e.g. Lokon). In the rest of the paper, we will use the data concerning the Feldspar sample to illustrate the contents of the database.

4. Contents of the database

4.1. SEM images

To give an indication of the shapes of the particles we provide one or two SEM images in the database per sample. By way of example Fig. 1 shows such an image for the Feldspar particles. Such images may, for example, be compared to images of particles collected directly from the atmosphere or in space [14] or be used for shape analyses, e.g. [15–19]. The one or two SEM images per sample in the database are not suited to infer detailed information about the sizes of the particles, mainly because they range over several orders of magnitude, in most cases, so that images with lower magnification will be biased towards showing only larger particles, and vice versa.

The particles in the Feldspar sample are irregularly shaped, like all of the sample particles at the creation of the database, except for the fly ash particles that consist of aggregates of spheres.

4.2. Particle composition and refractive indices

Samples of natural small particles are often composed of a variety of different minerals. Although the refractive indices at visible wavelengths of these constituent minerals may be known, the refractive index for the mixture may not be easy to derive from these values. To determine the quantitative mineral composition or the complex refractive index usually a bulk sample is needed, e.g. [20], and

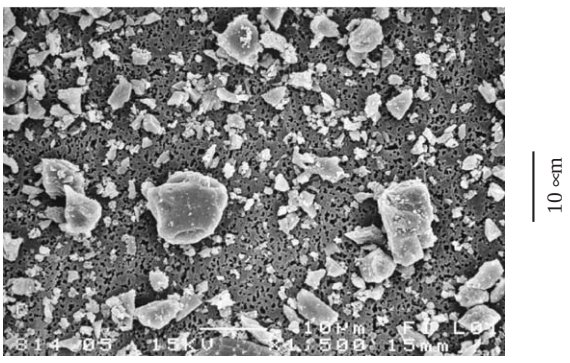

Fig. 1. SEM image of Feldspar particles. The particles are highly irregular in shape and show considerable differences in size. The scale of the figure is indicated by the bar on the right.

this is seldom available. For cases where the refractive index is not accurately known, we provide in the database a qualitative estimate of the mineral composition, and an estimate of the real part of the refractive index Re(m) based on values found in the literature for the constituent minerals. Less information is usually available for the imaginary part of the refractive index Im(m), because the natural variability within a mineral can be quite large. However, for silicates values at visible wavelengths mostly are in the range 10^{-2}–10^{-5} [21,22]. An indication of whether the value of Im(m) is relatively high or low is given by the color of the powdered sample, since white looking powders absorb little. The colors of the powders are shown on photographs included in the database.

For example, the main constituent minerals of the Feldspar sample are K-feldspar, plagioclase, and quartz as has been determined by means of an electron microprobe [23]. Therefore, Re(m) at 441.6 and 632.8 nm will be around 1.5–1.6. The light pink color of the Feldspar powder indicates that Im(m) will be relatively small.

4.3. Size distributions

Apart from shape and composition, size is a key property in determining the light scattering properties of small particles. For the samples of randomly oriented particles in the database, projected-surface-area distributions have been measured to determine the sizes of the particles using a Fritsch laser particle sizer [24] based on diffraction. Apart from projected-surface-area distributions expressed in radii of projected-surface-area-equivalent spheres r, we also provide number distributions and volume distributions as functions of radii of projected-surface-area-equivalent spheres r, because number distributions are often required for numerical applications and volume distributions are common in literature about atmospheric particles. To plot these three size distributions in a convenient way a change of variables from r to $\log r$ is often performed, so that three different types of size distributions are formed. In the database as well as in this paper $\log r$ always refers to r expressed in micrometers.

To characterize the sizes of the particles of a sample with a few parameters the effective radius r_{eff} (A.14) and effective standard deviation σ_{eff} (A.15) for projected-surface-area-equivalent spheres can be used. The use of different size definitions and size distributions is a potential source of confusion. Since for a proper use of the database a good understanding of this subject is indispensable, we give a more detailed discussion in Appendix A (see also [25, Section 7.1]).

In Fig. 2, we plot examples of the above-mentioned size distributions for the Feldspar sample. The shifts of the maxima of the number distribution $N(\log r)$, projected-surface-area distribution $S(\log r)$, and volume distribution $V(\log r)$ in Fig. 2 illustrate how each size distribution emphasizes a different size range. For example, the Feldspar particles have $r_{\text{eff}} = 1.0$ μm and $\sigma_{\text{eff}} = 1.0$. However, if we calculate the median radius (for projected-surface-area-equivalent spheres) for the volume distribution, we find a value of $\log r = 0.15$ which corresponds to $r = 1.4$ μm, i.e., 50% of the volume of the sample consists of particles with r smaller than 1.4 μm. Similarly, the projected-surface-area distribution yields a median radius of 0.73 μm ($\log r = -0.14$) and the number distribution a median radius of 0.3 μm ($\log r = -0.5$). Thus, for each application one should carefully consider which size distribution is most relevant.

In the database, we present normalized size distributions as they are given in Table 1 for the Feldspar sample, corresponding to the curves in Fig. 2. The number distribution $N(\log r)$, the projected-surface-area distribution $S(\log r)$, and the volume distribution $V(\log r)$ may be converted

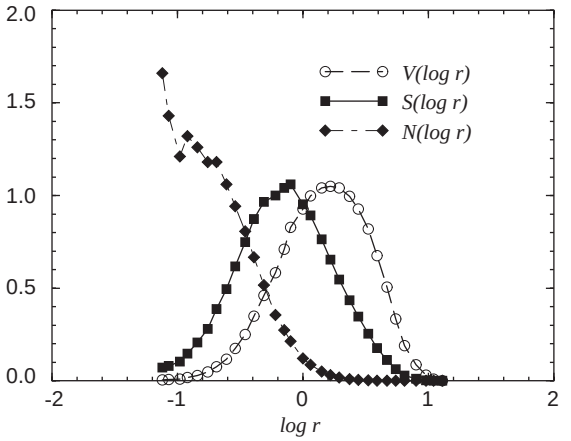

Fig. 2. Measured normalized projected-surface-area distribution $S(\log r)$, and corresponding normalized number $N(\log r)$ and volume distributions $V(\log r)$ of the Feldspar sample. The distributions are plotted as functions of $\log r$, where the radius of the projected-surface-area-equivalent sphere r is expressed in μm. The area under each curve equals unity.

to, respectively, the number distribution $n(r)$, the projected-surface-area distribution $s(r)$, and the volume distribution $v(r)$, by using Eqs. (A.17), (A.19), and (A.20). We note that some size distribution tables have been published in [26], but there $V(\log r)$ was normalized to 100% instead of 1.

As mentioned, the laser particle sizer we used is based on measurements of Fraunhofer diffraction patterns. The instrument determines the size distribution of a sample of particles suspended in a liquid. The resulting projected-surface-area distributions were obtained without assumptions about the refractive indices of the materials of the particles. According to the Instruction Manual of the particle sizer, experience has shown that results which are relatively correct and absolutely repeatable can be obtained down to a particle diameter of 0.2 μm. The uncertainties of the values of the projected-surface-area distribution $S(\log r)$ due to random (statistical) errors and systematic errors are not known, but we expect the relative uncertainties for the smallest particles in our samples to be larger than for particles with $r \simeq r_{\text{eff}}$.

The largest particle diameter that can be measured with the particle sizer is 2000 μm. However, the particles we are interested in are usually at least an order of magnitude smaller. In fact, the aerosol generator used in the light scattering experiments cannot handle samples containing a significant amount of particles larger than around 200 μm in diameter. Here, the statistical errors in $S(\log r)$ are expected to be relatively large compared with particles with $r \simeq r_{\text{eff}}$, because a small amount of large particles may contribute considerably to the projected surface area (and the volume).

In principle, relative uncertainties of $S(\log r)$ yield the same relative uncertainties in $N(\log r)$ and $V(\log r)$, because they are related by constants and factors of r only (Eqs. (A.21) and (A.22)). However, as shown in Fig. 2, $N(\log r)$ may be relatively large for the smallest measured particles, resulting in relatively large absolute errors. This should be kept in mind whenever the values of $N(\log r)$ in our database are used. In particular, if $S(\log r)$ is small but not known for say $r < r_0$ we cannot reliably extrapolate $N(\log r)$ for $r < r_0$ in figures like Fig. 2. Although the uncertainties of $S(\log r)$, $N(\log r)$, and $V(\log r)$ are not known, we have tabulated these functions in the database by numbers consisting of three figures to avoid rounding errors to accumulate in calculations involving these functions.

Table 1
Normalized number distribution $N(\log r)$, and corresponding normalized projected-surface-area distribution $S(\log r)$ and normalized volume distribution $V(\log r)$, of the Feldspar sample[a]

$\log r$	$N(\log r)$	$S(\log r)$	$V(\log r)$
−1.12	1.66E+00	7.29E−02	5.32E−03
−1.07	1.43E+00	8.04E−02	6.64E−03
−0.98	1.21E+00	1.04E−01	1.06E−02
−0.92	1.32E+00	1.48E−01	1.73E−02
−0.84	1.26E+00	2.07E−01	2.92E−02
−0.76	1.18E+00	2.81E−01	4.78E−02
−0.69	1.18E+00	3.87E−01	7.71E−02
−0.61	1.06E+00	4.96E−01	1.18E−01
−0.54	9.42E−01	6.17E−01	1.74E−01
−0.46	8.07E−01	7.49E−01	2.51E−01
−0.39	6.66E−01	8.73E−01	3.48E−01
−0.31	5.16E−01	9.65E−01	4.60E−01
−0.22	3.56E−01	1.00E+00	5.83E−01
−0.15	2.73E−01	1.04E+00	7.10E−01
−0.10	2.13E−01	1.06E+00	8.28E−01
0.00	1.22E−01	9.53E−01	9.26E−01
0.06	8.66E−02	8.93E−01	9.98E−01
0.15	5.00E−02	7.63E−01	1.04E+00
0.22	3.09E−02	6.55E−01	1.05E+00
0.29	1.84E−02	5.46E−01	1.04E+00
0.37	1.01E−02	4.36E−01	9.95E−01
0.44	5.87E−03	3.46E−01	9.26E−01
0.52	3.00E−03	2.55E−01	8.19E−01
0.59	1.50E−03	1.78E−01	6.75E−01
0.67	6.63E−04	1.12E−01	5.05E−01
0.74	2.64E−04	6.24E−02	3.34E−01
0.81	9.06E−05	2.99E−02	1.89E−01
0.90	2.26E−05	1.13E−02	8.77E−02
0.98	4.91E−06	3.45E−03	3.19E−02
1.04	9.22E−07	8.70E−04	9.30E−03
1.11	7.98E−08	1.05E−04	1.33E−03

[a]All three size distributions are functions of $\log r$, where r is expressed in μm.

5. Applications

There are several ways in which the data in the database can be useful. The data can be used in a direct manner, e.g. in comparisons with observations of light that has been scattered only once (see [4] and below) or to assess results of numerical light scattering methods for nonspherical particles [3,15,26]. Also, the data may be used in an indirect manner. For example, if a method is applied to extrapolate the measured angular distributions of the scattering matrix elements to the full scattering angle range, including forward and backward scattering, the extrapolated functions may serve as input for multiple scattering computations [9,27–30]. Another way to employ the data

in an indirect way, is to first find a fit to the experimental results, applying theoretical techniques using parameterized shape distributions. Then, the parameterized shape distribution constrained by the fit can be used to obtain the scattering and absorption properties at other scattering angles, wavelengths and/or sizes where experiments are impossible or not practical, e.g. in the middle and far infrared.

We like to note that a strong point of the database is that it provides *complete* scattering matrices as functions of the scattering angle and not one or two elements. This not only facilitates checking of systematic errors in the data, by e.g. applying "eye ball" tests or the Cloude test (e.g. [13]), but also makes it possible to perform multiple scattering calculations including polarization. Another advantage is that complete scattering matrices may help to obtain better constraints on the (model) shape parameters.

5.1. An example: comets

We give an example of the use of the database by comparing data in the database with results of Mie calculations. In addition, we compare these data with cometary observations of the degree of linear polarization as a function of the scattering angle.

The spectacular display of a bright comet is mostly caused by sunlight scattered by a cloud of micrometer-sized particles. Measurements of the brightness and polarization of this light potentially give information on the nature of these dust particles, if we know how to interpret these observations. The data from the database may play a key role in this interpretation process. Since infrared spectra have provided evidence for the presence of crystalline olivine in comets [31], we compare cometary observations with measured results of two cometary analogs in the database, i.e. a natural Mg-rich olivine sample (Olivine S) and a sample consisting mostly of iron-rich olivine particles obtained by grinding a piece of Allende meteorite (Allende) [4].

Fig. 3 shows measured matrix elements for a wavelength of 632.8 nm of Olivine S and Allende. These measured elements are compared with results of Mie calculations using the same wavelength and size distributions as for the measured data. The size distributions employed are given in the database. For the refractive index of Olivine S we chose $m = 1.62 - i10^{-5}$ based on experimental determinations for a similar sample in Jena [32]. For the Allende sample we chose $m = 1.65 - i10^{-2}$, based on data from the Jena optical constants database [33,34]. The comparison provides a compelling example of what has been noted many times before, namely, that results of Mie calculations for homogeneous spheres, in general, very poorly reproduce the scattering by irregular particles. In particular, it is interesting to note the large discrepancies between results of measurements and calculations for the element ratio $-F_{12}(\theta)/F_{11}(\theta)$, representing the degree of linear polarization for unpolarized incident light.

This element ratio is plotted again in Fig. 4, but now together with observations for comet Kobayashi–Berger–Milon, obtained with a filter with a width of 5 nm centered around 530 nm, and, at large scattering angles, observations of comet Halley, obtained using a wide band filter with a width of 108 nm centered around 686 nm [35]. These cometary observations are representative for a large group of comets, since cometary observations tend to compare fairly well, in particular at large scattering angles (small phase angles) [35,36]. The curves of the measurements and the observations are remarkably similar, which indicates that the olivine particles known to occur in comets may possess a similar degree of irregularity as the ones we used in the laboratory.

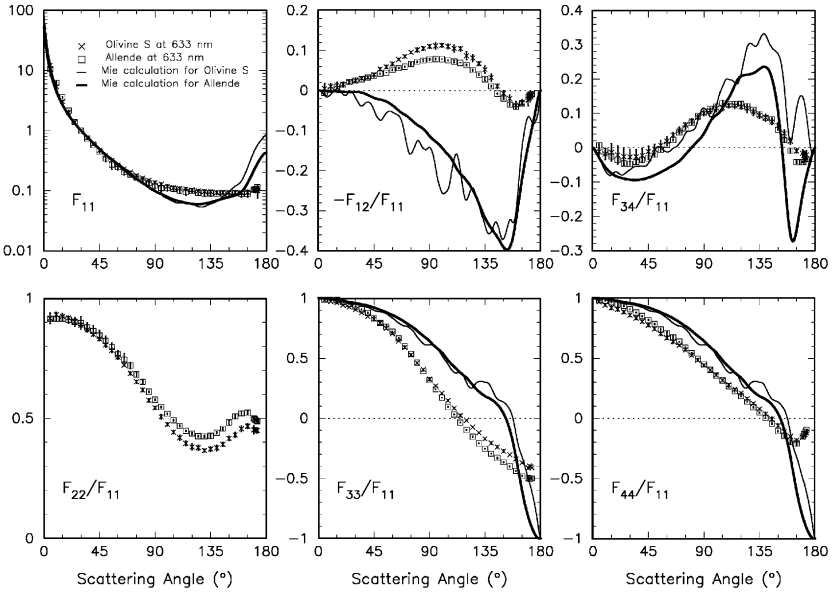

Fig. 3. Comparison of measured scattering matrix elements as functions of the scattering angle of Olivine S particles and Allende particles at 632.8 nm with results of Mie calculations for particles with the same size distributions and complex refractive indices as for the measured sample.

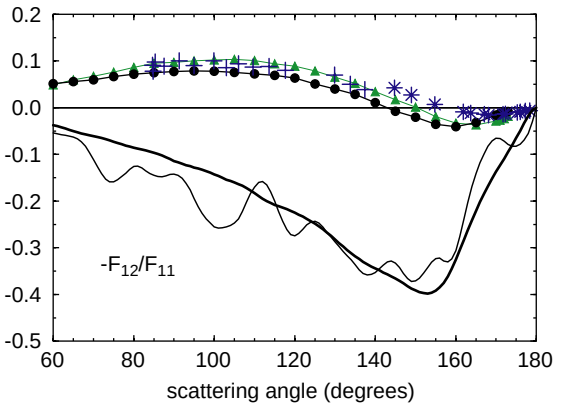

Fig. 4. The degree of linear polarization for unpolarized incident light as a function of the scattering angle of Olivine S particles (triangles) and Allende particles (circles) at 632.8 nm. Observations of comet Halley (asterisks) at 686 nm and comet Kobayashi–Berger–Milon (pluses) at 530 nm are also shown. In addition, results of Mie calculations for homogeneous spherical particles with the same size distributions and refractive index are included (thin solid line for Olivine S and thick solid line for Allende).

6. Discussion and conclusion

A large collection of light scattering data for irregular mineral particles is now available on the web. To choose data for a certain application, different selection criteria may be employed. For example, because of their origin and composition Pinatubo, Lokon, Sahara, and Loess possess a clear

relevance to studies of the Earth atmosphere, whereas the four Olivines and Allende are important for astronomical applications [4]. For comparison with numerical data, it may be convenient to select a sample for which not only the size distribution but also the refractive index is reasonably well known at 441.6 and 632.8 nm, such as the quartz sample, so that the number of free parameters is reduced [29]. Alternatively, one may want to select a sample for which the size range corresponds best to the size range appropriate for the numerical computations [15]. For other applications one may want to combine certain data to estimate in which domain the value of a specific light scattering property may lie [3]. In short, the information on sizes, shapes, composition, and refractive index in the database on the website may provide a basis for selecting scattering matrix data.

When applying the experimental data, one should bear in mind that because of their experimental origin, they have natural limitations. For example, measured projected-surface-area distributions can be converted to number distributions for use in light scattering calculations (see Appendix A). However, small absolute errors in the initial projected-surface-area distribution may cause large absolute errors in the resulting number distribution. See e.g. $S(\log r)$ and $N(\log r)$ near $\log r = -1$ in Fig. 2. Similarly, the error bars given for the matrix elements as functions of the scattering angle should preferably be taken into account for applications. For example, when comparing the data with results of light scattering computations one may include these error bars as weights in a least-squares fitting method.

It is difficult to adequately define and characterize the shapes of natural particles. Since no two irregular particles will be exactly the same, a statistical description will be most practical. Many different descriptions are possible, see e.g. [15,19], each with its own advantages and disadvantages. The irregularity in shape often inhibits a proper quantitative determination of the particle composition and refractive index. Also the determination of the size distribution of the particles may be affected by the shape of the particles [24]. Despite these difficulties, the enormous advantage of studying experimental light scattering by natural particles is that we gain insight into realistic scattering behavior, even though the difficulty in characterizing the particles may limit the interpretation of the data. The database constitutes a state-of-the-art overview of our measured scattering matrices of irregular particles and their particle characteristics. We hope that this extensive collection of information will be used for many applications and trigger further research.

We plan to update this database regularly with new light scattering matrices for various samples of particles.

Acknowledgements

We are indebted to the many people who helped us to obtain the mineral samples, in particular, K. Lumme, J.P. Lunkka, G. Kuik, F.S. Rondonuwu, D. Heymann, R.D. Schuiling, R.A. West, and A.D. Clarke. We are grateful to E. Rol and J. Bouma for aid with the measurements and technical support, and to M. Konert for measuring the size distribution of the samples. It is a pleasure to thank M.I. Mishchenko for many fruitful discussions. Also, we like to thank D. Stam, and B. Veihelmann for testing a preliminary version of the website. This experimental work on light scattering is part of the research program of the Foundation for Fundamental Research on Matter and is financially supported by NWO. Additional financial support has been obtained through an NWO Pionier grant of Waters and from the Netherlands Research School for Astronomy, NOVA. This work was also supported by Contract AYA2001-1177.

Appendix A.

The main purpose of this appendix is to provide definitions and interrelations for the size distributions used in the database.

A.1. Number distributions

Consider a collection of randomly oriented particles with arbitrary shapes. Replace each particle by a sphere having the same average (over all orientations) projected surface area. This creates a collection of spheres which we shall call projected-surface-equivalent spheres or briefly spheres in this appendix. Let r denote the radius of such a sphere. We introduce a function $v(r)$ so that $v(r)\,\mathrm{d}r$ is the number of spheres per unit volume (of space) having radii between r and $r+\mathrm{d}r$. Thus, the number of spheres per unit volume with radii between r_1 and r_2 is given by $\int_{r_1}^{r_2} v(r)\,\mathrm{d}r$. Units of $v(r)$ are, e.g. $\mu\mathrm{m}^{-1}\ \mathrm{cm}^{-3}$.

The total number of spheres per unit volume is

$$\mathtt{N} = \int_0^\infty v(r)\,\mathrm{d}r. \tag{A.1}$$

Units of $\mathtt{N}$ are for example cm^{-3}. We shall call $v(r)$ a number distribution (function) and

$$n(r) = v(r)/\mathtt{N}, \tag{A.2}$$

a normalized number distribution of the collection of particles. Units for the latter are, e.g. $\mu\mathrm{m}^{-1}$. Hence $n(r)\,\mathrm{d}r$ is the fraction of the total number of particles per unit volume having radii between r and $r+\mathrm{d}r$. Consequently, the relative contribution of spheres with radii between r_1 and r_2 to the total number of particles per unit volume can be written as

$$\frac{\int_{r_1}^{r_2} v(r)\,\mathrm{d}r}{\mathtt{N}} = \int_{r_1}^{r_2} n(r)\,\mathrm{d}r. \tag{A.3}$$

Note that this quantity is dimensionless and can be expressed in percent.

Obviously, we have

$$\int_0^\infty n(r)\,\mathrm{d}r = 1, \tag{A.4}$$

which, in practice, gives a handy test for a normalized number distribution $n(r)$.

A.2. Volume distributions

The total volume occupied by the (projected-surface-area-equivalent) spheres per unit volume of space is

$$\mathtt{V} = \int_0^\infty v(r)\left(\frac{4}{3}\pi r^3\right)\mathrm{d}r. \tag{A.5}$$

Units of V are, e.g. $\mu m^3\,cm^{-3}$. The relative contribution to this by spheres with radii between r_1 and r_2 is dimensionless and given by $\int_{r_1}^{r_2} v(r)\,dr$, where the normalized volume distribution of the collection of particles

$$v(r) = \frac{v(r)(4/3)\pi r^3}{\mathrm{V}}. \tag{A.6}$$

Units of $v(r)$ are, e.g. μm^{-1}. A handy test is provided by

$$\int_0^\infty v(r)\,dr = 1. \tag{A.7}$$

A.3. Projected-surface-area distributions

We can define projected-surface-area distributions analogous to volume distributions. Thus, the relative contribution to the total surface area of projected-surface-area-equivalent spheres with radii between r_1 and r_2 per unit volume of space is the dimensionless quantity

$$\frac{\int_{r_1}^{r_2} v(r)\pi r^2\,dr}{\int_0^\infty v(r)\pi r^2\,dr} = \frac{\int_{r_1}^{r_2} v(r)\pi r^2\,dr}{\mathrm{S}} = \int_{r_1}^{r_2} s(r)\,dr, \tag{A.8}$$

where S (in units of, for instance, $\mu m^2\,cm^{-3}$) is the total projected surface area occupied by the spheres per unit volume of space and the normalized projected-surface-area distribution of the collection of particles

$$s(r) = \frac{v(r)\pi r^2}{\mathrm{S}} = \frac{v(r)r^2}{\int_0^\infty v(r)r^2\,dr}. \tag{A.9}$$

Units of $s(r)$ are, e.g. μm^{-1}. A handy test is provided by

$$\int_0^\infty s(r)\,dr = 1. \tag{A.10}$$

Note that all three functions $n(r)$, $v(r)$, and $s(r)$ are normalized size distributions of a particular collection of arbitrary particles in random orientation.

A.4. Interrelations for the size distributions

According to Eqs. (A.2), (A.6), and (A.9) we have the normalized number distribution

$$n(r) = v(r)/\mathrm{N}, \tag{A.11}$$

the normalized volume distribution

$$v(r) = c_1 r^3 n(r) \quad \text{with } c_1 = \frac{4}{3}\pi\frac{\mathrm{N}}{\mathrm{V}} \tag{A.12}$$

and the normalized projected-surface-area distribution

$$s(r) = c_2 r^2 n(r) \quad \text{with } c_2 = \pi\frac{\mathrm{N}}{\mathrm{S}}. \tag{A.13}$$

If one of the functions $n(r)$, $v(r)$, or $s(r)$ is given we can find the other two from Eqs. (A.11), (A.12), and (A.13) apart from constants, but these constants can be found directly from the normalization conditions expressed by Eqs. (A.4), (A.7), and (A.10). In studies of light scattering, the projected surface area is very important. Therefore, the so-called effective radius is often used [37]. This is given by

$$r_{\mathrm{eff}} = \frac{\int_0^\infty r\pi r^2 n(r)\,\mathrm{d}r}{\int_0^\infty \pi r^2 n(r)\,\mathrm{d}r} = \frac{3}{4}\frac{\mathrm{V}}{\mathrm{S}} = \int_0^\infty rs(r)\,\mathrm{d}r, \tag{A.14}$$

which shows that $s(r)$ is the weighting function here. To characterize size distributions with a few parameters, this effective radius and the effective standard deviation or the effective variance can conveniently be used. The effective standard deviation is defined as

$$\sigma_{\mathrm{eff}} = \sqrt{\frac{\int_0^\infty (r - r_{\mathrm{eff}})^2 \pi r^2 n(r)\,\mathrm{d}r}{r_{\mathrm{eff}}^2 \int_0^\infty \pi r^2 n(r)\,\mathrm{d}r}} = \sqrt{\frac{\int_0^\infty (r - r_{\mathrm{eff}})^2 s(r)\,\mathrm{d}r}{r_{\mathrm{eff}}^2 \int_0^\infty s(r)\,\mathrm{d}r}}. \tag{A.15}$$

The effective variance v_{eff} equals σ_{eff}^2. When the sizes of the particles are considered relative to the wavelength λ of the scattered light the effective size parameter $x_{\mathrm{eff}} = 2\pi r_{\mathrm{eff}}/\lambda$ can be employed. However, values for the effective radius and the effective standard deviation may be misleading if the size distribution is, for example, bimodal. In such a case other or more parameters are needed to describe the size distributions in a satisfactory way.

A.5. Plots

In plots we may like to use $\log r$, where r is expressed in micrometers instead of r as the abscissa, especially when the range of r is very large. As an example we consider $n(r)$. If we plot $n(r)$ versus $\log r$ we loose the simple interpretation of areas under the curve as relative number of particles in a certain size range (see Eq. (A.3)). But we can change the variable and define a new function $N(\log r)$ so that $N(\log r)\,\mathrm{d}\log r$ is the relative number of spheres per unit volume (of space) in the size range $\log r$ to $\log r + \mathrm{d}\log r$. So

$$\int_{r_1}^{r_2} n(r)\,\mathrm{d}r = \int_{\log r_1}^{\log r_2} N(\log r)\,\mathrm{d}\log r = \int_{r_1}^{r_2} \left[N(\log r)\frac{\mathrm{d}\log r}{\mathrm{d}r}\right]\mathrm{d}r = \int_{r_1}^{r_2} \frac{N(\log r)}{r\ln 10}\,\mathrm{d}r, \tag{A.16}$$

where $\ln 10$ is the natural logarithm of 10. Consequently,

$$N(\log r) = \ln 10 rn(r) = 2.303 rn(r). \tag{A.17}$$

Eq. (A.16) shows that it is advantageous to plot $N(\log r)$ versus $\log r$ or in other words $\ln 10 rn(r)$ versus $\log r$, because we can use the area rule again, i.e., equal areas under parts of the curve means equal relative amounts of spheres per unit volume in the ranges considered. In the literature cumulative size distributions, such as the cumulative number distribution $n_{\mathrm{c}}(r)$, are frequently encountered. Here $n_{\mathrm{c}}(r)$ is the fraction of particles per unit volume with radii smaller than r, i.e., $n_{\mathrm{c}}(r) = \int_0^r n(r')\,\mathrm{d}r'$ yielding for use in plots

$$\frac{\mathrm{d}n_{\mathrm{c}}(r)}{\mathrm{d}\log r} = \ln 10 rn(r) = N(\log r). \tag{A.18}$$

So far we have considered $n(r)$, but we can do the same for all absolute or relative (normalized) distribution functions (see Fig. 2). Thus, we define

$$S(\log r) = \ln 10 rs(r) = 2.303 rs(r), \tag{A.19}$$

$$V(\log r) = \ln 10 rv(r) = 2.303 rv(r). \tag{A.20}$$

It should be noted that $N(\log r)$, $S(\log r)$, and $V(\log r)$ are dimensionless functions which are also called size distributions. For normalized distributions one often omits the factor 2.303 and performs the normalization by integration of the resulting curve over the entire range (the total area under the curve).

A useful relation, that follows from using Eqs. (A.12)–(A.14) and Eqs. (A.19)–(A.20) is

$$\frac{S(\log r)}{V(\log r)} = \frac{s(r)}{v(r)} = \frac{c_2}{c_1 r} = \frac{r_{\text{eff}}}{r}. \tag{A.21}$$

Thus, $s(r_{\text{eff}}) = v(r_{\text{eff}})$ and $S(\log r_{\text{eff}}) = V(\log r_{\text{eff}})$. For this reason the curves for $S(\log r)$ and $V(\log r)$ plotted versus $\log r$ intersect at $\log r_{\text{eff}}$. Consequently, r_{eff} can be quickly estimated from figures like Fig. 2 or tables like Table 1 in the database. Furthermore, we have $S(\log r) > V(\log r)$ if $\log r < \log r_{\text{eff}}$ and $S(\log r) < V(\log r)$ if $\log r > \log r_{\text{eff}}$ as can be seen in Fig. 2.

Similarly, Eq. (A.13) gives in combination with Eqs. (A.17) and (A.19)

$$\frac{N(\log r)}{S(\log r)} = \frac{n(r)}{s(r)} = \frac{1}{c_2 r^2} = \frac{\mathtt{S}}{\pi \mathtt{N}} \frac{1}{r^2}. \tag{A.22}$$

So the curves for $N(\log r)$ and $S(\log r)$ intersect at $\log r = \log\sqrt{\mathtt{S}/\pi\mathtt{N}}$ and $N(\log r) > S(\log r)$ if $\log r < \log\sqrt{\mathtt{S}/\pi\mathtt{N}}$ and $N(\log r) < S(\log r)$ if $\log r > \log\sqrt{\mathtt{S}/\pi\mathtt{N}}$.

References

[1] Hovenier JW. Measuring scattering matrices of small particles at optical wavelengths. In: Mishchenko MI, Hovenier JW, Travis LD, editors. Light scattering by nonspherical particles. San Diego: Academic Press; 2000. p. 355–65.

[2] Hovenier JW, Volten H, Muñoz O, Van der Zande WJ, Waters LBFM. Laboratory studies of scattering matrices for randomly oriented particles. Potentials, problems, and perspectives. J Quant Spectrosc Radiat Transfer 2003;79–80:741–55.

[3] Volten H, Muñoz O, Rol E, de Haan JF, Vassen W, Hovenier JW, Muinonen K, Nousiainen T. Scattering matrices of mineral particles at 441.6 nm and 632.8 nm. J Geophys Res 2001;106:17,375–401.

[4] Muñoz O, Volten H, de Haan JF, Vassen W, Hovenier JW. Experimental determination of scattering matrices of olivine and Allende meteorite particles. Astron Astrophys 2000;360:777–88.

[5] Muñoz O, Volten H, de Haan JF, Vassen W, Hovenier JW. Experimental determination of scattering matrices of randomly oriented fly ash and clay particles at 442 and 633 nm. J Geophys Res 2001;106:22,833–44.

[6] Muñoz O, Volten H, de Haan JF, Vassen W, Hovenier JW. Experimental determination of the phase function and degree of linear polarization of El Chichon and Pinatubo volcanic ashes. J Geophys Res 2002;107:10.1029/2001JD000983.

[7] Muñoz O, Volten H, Hovenier JW. Experimental light scattering matrices relevant to cosmic dust. In: Videen G, Kocifaj M, editors. Optics of cosmic dust. Dordrecht: Kluwer Academic Publishers; 2002.

[8] Mishchenko MI, Travis LD, Lacis AA. Scattering, absorption, and emission of light by small particles. Cambridge: Cambridge University Press; 2002.

[9] Veihelmann B, Volten H, van der Zande WJ. Simulations of light reflected by an atmosphere containing irregularly shaped mineral aerosol over the ocean. Geophys Res Lett 2004;31:10.1029/2003GL018229.

[10] Van de Hulst HC. Light scattering by small particles. New York: Wiley; 1957.
[11] Hovenier JW, van der Mee CVM. Fundamental relationships relevant to the transfer of polarized light in a scattering atmosphere. Astron Astrophys 1983;128:1–16.
[12] Hovenier JW, Van de Hulst HC, van der Mee CVM. Conditions for the elements of the scattering matrix. Astron Astrophys 1986;157:301–10.
[13] Hovenier JW, van der Mee CVM. Testing scattering matrices, a compendium of recipes. J Quant Spectrosc Radiat Transfer 1996;55:649–61.
[14] Warren JL, Zolensky ME, Thomas K, Dodson AL, Watts LA, Wentworth S. Cosmic dust catalog 15. Houston: NASA; 1997.
[15] Nousiainen T, Muinonen K, Räisänen P. Scattering of light by large Saharan dust particles in a modified ray-optics approximation. J Geophys Res 2003;108:10.1029/2001JD001277.
[16] Hill SC, Hill AC, Barber PW. Light scattering by size/shape distributions of soil particles and spheroids. Appl Opt 1984;23:1025–31.
[17] Jalava JP, Taavitsainen VM, Lamberg L, Haario H. Determination of particle and crystal size distribution from turbidity spectrum of TiO_2 pigment by means of T-matrix. J Quant Spectrosc Radiat Transfer 1998;60:399–409.
[18] Koren I, Ganor E, Joseph JH. On the relation between size and shape of desert dust aerosol. J Geophys Res 2001;106:18,047–54.
[19] Riley CM, Rose WI, Bluth GJS. Quantitative shape measurements of distal volcanic ash. J Geophys Res 2003;108:10.1029/2001JB000818.
[20] Dorschner J, Begemann B, Henning Th, Jäger C, Mutschke H. Steps towards interstellar silicate mineralogy, II. Study of Mg–Fe–silicate glasses of variable composition. Astron Astrophys 1995;300:503–20.
[21] Egan WG, Hilgeman TW. Optical properties of inhomogeneous materials: applications to geology, astronomy, chemistry, and engineering. New York: Academic Press; 1979.
[22] Gerber HE, Hindman EE, editors. Light absorption by aerosol particles. In: Technical Proceedings of the First International Workshop on Light Absorption by Aerosol Particles, Fort Collins, CO, 1980. Hampton, VA: Spectrum; 1982.
[23] Reed SJB. Electron microprobe analysis. Cambridge: Cambridge University Press; 1993.
[24] Konert M, Vandenberghe J. Comparison of laser grain size analysis with pipette and sieve analysis: a solution for the underestimation of the clay fraction. Sedimentology 1997;44:532–5.
[25] Seinfeld JH, Pandis SN. Atmospheric chemistry and physics: from air pollution to climate change. New York: Wiley; 1998.
[26] Volten H. Light scattering by small planetary particles: an experimental study. PhD thesis, Free University, Amsterdam; 2001.
[27] Moreno F, Muñoz O, Lopez-Moreno JJ, Molina A, Ortiz JL. A Monte Carlo code to compute energy fluxes in cometary nuclei. Icarus 2002;156:474–84.
[28] Braak CJ, de Haan JF, van der Mee CVM, Hovenier JW, Travis LD. Parameterized scattering matrices for small particles in planetary atmospheres. J Quant Spectrosc Radiat Transfer 2001;69:585–604.
[29] Liu L, Mishchenko MI, Hovenier JW, Volten H, Muñoz O. Scattering matrix of quartz aerosols: comparison and combination of laboratory and Lorenz-Mie results. J Quant Spectrosc Radiat Transfer 2003;79–80:911–20.
[30] Mishchenko MI, Geogdzhaev I, Liu L, Orgen A, Lacis A, Rossow W, Hovenier JW, Volten H, Muñoz O. Aerosol retrievals from AVHRR radiances: effects of particle nonsphericity and absorption and an updated long-term global climatology of aerosol properties. J Quant Spectrosc Radiat Transfer 2003;75–80:953–72.
[31] Crovisier J, Leech K, Bockele-Morvan D, Brooke TY, Hanner MS, Altieri B, Keller HU, Lellouch E. Observed with the infrared space observatory at 2.9 astronomical units from the sun. Science 1997;275:1904–7.
[32] Fabian D, Henning T, Jäger C, Mutschke H, Dorschner J, Werhan O. Steps toward interstellar silicate mineralogy VI. Dependence of crystalline olivine IR spectra on iron content and particle shape. Astron Astrophys 2001;378:228–38.
[33] Henning T, Il'In VB, Krivova NA, Michel B, Voshchinnikov NV. WWW database of optical constants for astronomy. Astron Astrophys 1999;136(Suppl):405–6.
[34] Jäger C, Il'In VB, Henning T, Mutschke H, Fabian D, Semenov DA, Voshchinnikov NV. A database of optical constants of cosmic dust analogs. J Quant Spectrosc Radiat Transfer 2003;79–80:765–74.

[35] Chernova GP, Kiselev NN, Jockers K. Polarimetric characteristics of dust particles as observed in 13 comets: comparison with asteroids. Icarus 1993;103:144–58.
[36] Levasseur-Regourd AC, Hadamcik E, Renard JB. Evidence for two classes of comets from their polarimetric properties at large phase angles. Astron Astrophys 1996;313:327–33.
[37] Hansen JE. Travis LD. Light scattering in planetary atmospheres. Space Sci Rev 1974;16:527–610.